JOURNAL OF GEOPHYSICAL RESEARCH, VOL. 99, NO. A12, PAGES 23,661–23,671, DECEMBER 1, 1994

Electron number density fluctuations near the plasmapause observed by the CRRES spacecraft

M. J. LeDocq, D. A. Gurnett, and R. R. Anderson
Department of Physics and Astronomy, University of Iowa, Iowa City

Abstract. Large quasi-periodic fluctuations in the electron number density are often encountered near and inside the plasmapause by the CRRES satellite. A power spectral analysis reveals electron density fluctuations with frequencies ranging from 2 mHz to approximately 61 mHz. Plasma density irregularities in the outer plasmasphere sometimes have power spectral slopes near −5/3, which suggest the presence of well-developed two-dimensional magnetohydrodynamic turbulence. Quasi-periodic fluctuations have been found outside the plasmasphere with spatial scales along the orbit path of approximately 750 km. A statistical analysis shows that the density fluctuation amplitudes are largest between $L = 3$ and $L = 6$, the region in which the plasmapause is located. The density fluctuation amplitudes decrease with increasing L shell for $L > 6$. Normalized fluctuation amplitudes greater than 10% are found in only 25% of the available data of this study. A significant magnetic local time dependence cannot be found due to incomplete data availability during the 9.00 to 14.99 MLT and the 15.00 to 20.99 MLT sectors.

1. Introduction

Small-scale plasma density fluctuations are studied by using plasma wave observations from the Combined Release and Radiation Effects Satellite (CRRES). This spacecraft provides measurements near the equatorial plane at radial distances extending out to about 6.3 R_E (Earth radii). Several previous spacecraft, most notably OGO 5, GEOS 1, and GEOS 2, have provided plasma density measurements in this same region. The plasma density measurements made by the light ion mass spectrometer on OGO 5 had a time resolution of 4 s [*Harris and Sharp*, 1969]. The OGO 5 data showed large density fluctuations near the plasmapause in the bulge region after periods of enhanced fluctuating geomagnetic activity [*Chappell et al.*, 1970; *Carpenter and Chappell*, 1973]. The relaxation sounder experiments on board GEOS 1 and GEOS 2 produced electron density measurements once every 22 s in the routine operating mode, or once every 86 ms in the f_{pe} tracking mode [*Higel*, 1978; *Higel and Lei*, 1984]. The GEOS 1 data showed density fluctuations with periods of 3–4 min at some plasmapause crossings. GEOS 1 also observed fluctuations with amplitudes of 1–3% and periods of approximately 10 s in other regions of the magnetosphere [*Higel*, 1978], although no in-depth study of density fluctuations was undertaken.

Other types of density structures also occur near the plasmapause. Longitudinal ripples in the dayside plasmapause with peak-to-peak amplitudes of up to 0.4 R_E were identified in early whistler studies of the plasmapause [*Carpenter*, 1966; *Angerami and Carpenter*, 1966; *Park and Carpenter*, 1970], and ripplelike plasma density structures were also encountered by the OGO 5 satellite [*Chappell*, 1972]. *Chappell* [1972] proposed that structures of this type could be detached plasma regions that peel off from the plasmasphere on the dayside and eventually corotate to the evening-dusk sector. Other studies of the OGO 5 data [*Chappell et al.*, 1971; *Chappell*, 1974] have found these detached regions to be located most often in the afternoon-dusk sector and less often in the dayside sector. Similar structures were also observed by the S^3-A satellite [*Maynard and Cauffman*, 1973]. Further studies have interpreted similar density structures as plasmatails that are formed in the bulge region and then wrap longitudinally around the main plasmapause [*Chen and Wolf*, 1972]. Models using various electric field configurations have had some success in producing behavior resembling the characteristics of detached plasma regions and small-scale density irregularities detected by whistlers and satellite-borne experiments [*Chen and Wolf*, 1972; *Chen and Grebowsky*, 1974; *Grebowsky and Chen*, 1976].

Small-scale quasi-periodic fluctuations in electron number density are frequently observed near the plasmapause by the plasma wave instrument on the CRRES spacecraft. The high-resolution density data provided by the CRRES plasma wave instrument make it possible to study the characteristics of density irregularities with amplitudes and scale lengths that are small compared to the thickness of the plasmapause. Also, the large size of the data set makes a statistical analysis of the location of the density irregularities possible.

2. CRRES Spacecraft and Data Handling

The plasmapause is the outer boundary of the plasmasphere and is characterized by a sharp decrease in plasma density between the high-density plasmasphere and the low-density plasma of the magnetosphere outside the plasmasphere. The CRRES spacecraft remains in or near the plasmasphere during its entire orbit and provides high time resolution electron number density data near the plasmapause twice per orbit. This section of the paper describes the CRRES orbit, the plasma wave instrumentation, and the procedures used to produce electron density values.

Paper number 94JA02294.
0148-0227/94/94JA-02294$05.00

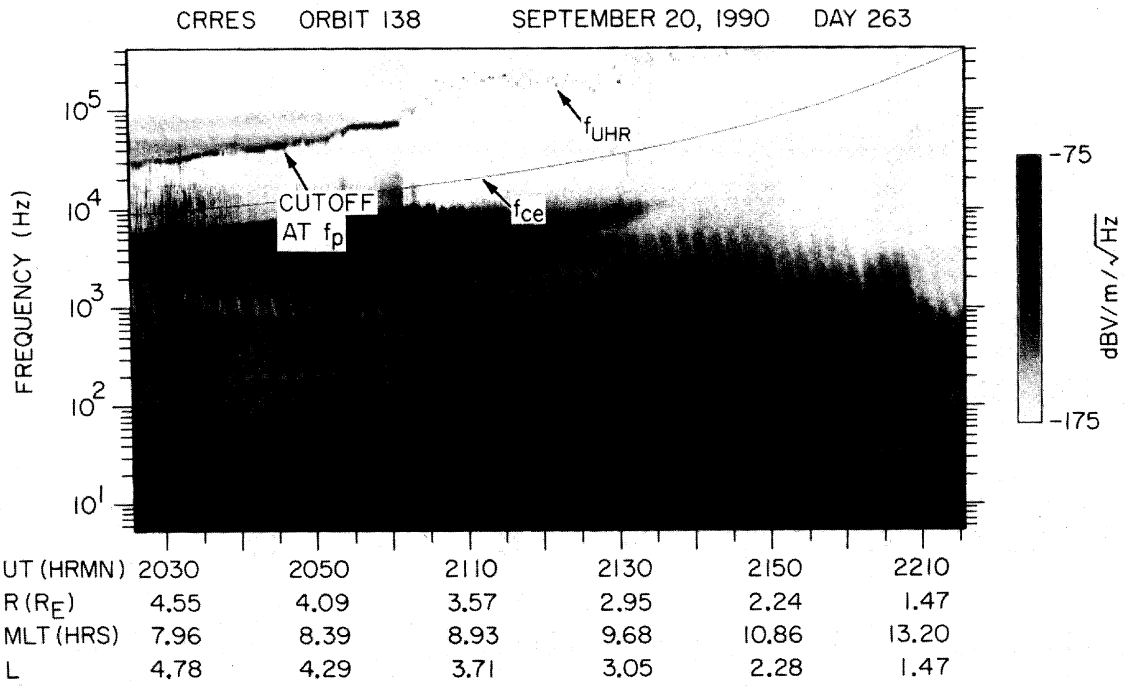

Figure 1. A frequency-time spectrogram of data from the CRRES Plasma Wave Experiment sweep frequency receiver for the time interval from 2026:02 UT to 2215:08 UT, September 20, 1990, during the inbound portion of orbit 138.

CRRES Orbit Parameters and Plasma Wave Instrument

The CRRES spacecraft was launched on July 25, 1990 [*Johnson and Kierein*, 1992], into an elliptical Earth orbit with an initial perigee altitude of 350 km and an apogee geocentric radial distance of 6.3 R_E. The orbit has an inclination of 18.2°, a period of 9 hours 52 min, and an initial magnetic local time at apogee of 0800 [*Anderson et al.*, 1992].

The CRRES Plasma Wave Experiment includes a spectrum analyzer that produces high-time-resolution electric field spectra in the frequency range from 5 Hz to 10 kHz and a sweep frequency receiver (SFR) that produces high-frequency-resolution electric field spectra in the frequency range from 100 Hz to 400 kHz [*Anderson et al.*, 1992]. The sweep frequency receiver measurements are obtained in four frequency bands with 32 steps per band. Band 1 (100–800 Hz) produces one spectrum per 32 s. Band 2 (800 Hz to 6.4 kHz) produces one spectrum per 16 s. Band 3 (6.4–50 kHz) and Band 4 (50–400 kHz) are sampled at a rate of 4 steps/s each and produce one spectrum every 8 s. The electron number density is calculated from narrow-band emissions at the upper hybrid resonance frequency, f_{UHR} [*Mosier et al.*, 1973], and from the cutoff at the plasma frequency, f_p, of continuum radiation [*Gurnett and Frank*, 1974]. Because these emissions usually occur in bands 3 and 4, electron number density values are normally produced every 8 s. This sampling rate is higher than that produced by previous spacecraft and allows the study of density fluctuations with periods as small as 16 s. Figure 1 shows a spectrogram produced by the CRRES plasma wave experiment during an inbound plasmapause crossing on September 20, 1990, from 2026:02 UT to 2215:08 UT. Universal time is plotted along the horizontal axis. The horizontal scale also provides the spacecraft coordinates such as the geocentric radial distance in units of Earth radii, the McIlwain L parameter, and the magnetic local time (MLT) in hours. The highest-intensity emissions are represented by black, and the lowest-intensity emissions are represented by white. Frequencies from 5 Hz to 400 kHz are plotted logarithmically on the vertical scale. The 5-Hz to 100-Hz portion of the spectrogram is derived from the spectrum analyzer, and the 100-Hz to 400-kHz portion is produced by the sweep frequency receiver. The electron cyclotron frequency, which is proportional to the magnetic field strength, is plotted as the solid curve across the spectrogram.

Computation of the Electron Number Density

Narrow-band upper hybrid resonance emissions are often detected in the plasmasphere and often make a smooth transition to a cutoff of continuum radiation emissions at the electron plasma frequency outside the plasmapause [*Shaw and Gurnett*, 1975]. These emissions are frequently observed in the CRRES spectrograms and provide a useful method of calculating the electron number density. The plasma frequency cutoff of continuum radiation is present from approximately 2026 UT to 2101 UT in the upper portion of the spectrogram in Figure 1. The cutoff frequency makes a smooth transition to emissions at the upper hybrid resonance frequency at approximately 2101 UT. A computer program allows these emissions to be traced by hand. To trace the

emissions, the spectrogram is displayed on the computer screen in an expanded format, and a mouse and pointer are used to digitize the frequency of upper hybrid emissions inside the plasmapause and cutoffs at the electron plasma frequency outside the plasmapause. The computer program used to digitize the spectrogram information also calculates the electron number density.

The electron plasma frequency is given by

$$f_p = \frac{1}{2\pi}\left[\frac{n_e e^2}{\varepsilon_0 m_e}\right]^{1/2} \tag{1a}$$

or

$$f_p \simeq 8.98(n_e)^{1/2} \text{ kHz} \tag{1b}$$

where n_e is the electron number density, e is the electron charge, m_e is the electron mass, and ε_0 is the permittivity of free space. Equation (1b) gives the plasma frequency in kilohertz when the electron number density is given in electrons per cubic centimeter. The upper hybrid resonance frequency is given by

$$f_{\text{UHR}} = (f_{\text{ce}}^2 + f_p^2)^{1/2} \tag{2}$$

where the electron cyclotron frequency, f_{ce}, is given by

$$f_{\text{ce}} = \frac{eB}{2\pi m_e} \tag{3a}$$

or

$$f_{\text{ce}} \simeq 2.8 \times 10^6 B \text{ Hz} \tag{3b}$$

where B is the magnetic field strength. The units of f_{ce} in equation (3b) are hertz when the magnetic field strength has units of gauss. The magnetic field is measured by the flux gate magnetometer on board the CRRES spacecraft [*Singer et al.*, 1992], and these data are used to calculate the electron cyclotron frequency. The electron number density is calculated directly from equation (1b) or (2). When the plasma frequency has been traced, the electron number density, with units of electrons per cubic centimeter, is calculated by using equation (1b), where f_p is in kilohertz. When the upper hybrid resonance frequency is traced, the number density is calculated by using equation (2), where f_{UHR} and f_{ce} are in kilohertz. Once the spectrograms have been traced, the resulting electron number density data files can then be analyzed by using procedures that will be discussed in sections 3 and 4.

Error Analysis of Tracing Procedure

Several sources of uncertainty are present in the determination of the upper hybrid and plasma frequencies during the tracing procedure. The uncertainties can be categorized as instrument noise, noise due to the characteristics of the upper hybrid and plasma frequency emissions profiles, and error due to human interpretation of the tracing procedure. The instrument noise is negligible compared to the other two sources. Upper hybrid and plasma frequency emissions are often detected in several frequency channels during a given 8.192-s sweep interval. This spread in frequency introduces errors in the tracing procedure. In most cases it is appropriate to choose the pixel that represents the frequency channel with the most intense emission. Where continuum radiation is clearly present, it is usually appropriate to choose the frequency at which the cutoff of the emission occurs. Sometimes, time periods occur where there is no clear indication of the correct choice of frequency channel using the above guidelines. In such cases the individual making the trace must determine the correct frequency by inference of the behavior of the emissions that occur immediately before and after this time period. Therefore each trace contains uncertainties due to the inherent thickness of the upper hybrid emission line or the plasma frequency cutoff and due to human interpretation of the profile. These two sources of uncertainty are not easily distinguishable, and both contribute to the error spectrum.

The spectral analysis, described in the next section, examines the power spectra of selected density profiles. These spectra are produced by performing a fast Fourier transform on the density time series and plotting the squares of the Fourier coefficients versus frequency. The error spectrum introduced by the tracing procedure can be evaluated by taking the difference of two traces of the same time period. The power spectrum of the difference of the two traces is assumed to be the error spectrum for this time series and contains all of the sources of uncertainty discussed above. The power spectrum is considered to be reliable only in the frequency range where the level of the power spectrum is greater than the level of the error spectrum. The power spectra and error spectra included in this analysis usually have amplitudes that are comparable for frequencies greater than 30–40 mHz. Therefore all conclusions of this paper are based on spectral components with frequencies less than 30–40 mHz.

One other potential source of error should also be discussed, error in the electron density spectrum due to variation in the times at which the upper hybrid profile intersects the SFR sweep. Density values are determined when the SFR sweeps across the frequency channel in which the upper hybrid or plasma frequency emission occurs. As the f_{UHR} or f_p emissions fluctuate, they are observed in different frequency channels during successive sweeps. The sampling is then not regularly spaced in time. The nonuniform sampling thereby introduces an error in the power spectrum. In order to find the error in the time interval between data values, the maximum change $\Delta f/f$ between consecutive upper hybrid frequency values was found during the time periods being analyzed. When $\log f = \beta t$ was used as an approximate representation of the SFR sweep, it was found that the maximum error in data spacing is $\Delta t/T \cong 0.035$, where $T = 8.192$ s is the sweep period. It can be shown analytically that this error has a negligible effect on the power spectrum. As a specific test of the effect of nonuniform sampling on the power spectrum, random errors of magnitude $-\Delta t \leq t \leq +\Delta t$ were introduced into the time series. The power spectra found for the modified time series did not differ significantly from the power spectra of the original time series.

3. Spectral Analysis of Density Fluctuations

Analysis Procedure

Electron density profiles are plotted by using the values calculated from the tracing program. For example, the density profile produced by tracing the upper hybrid emission from the spectrogram in Figure 1 is plotted as the upper

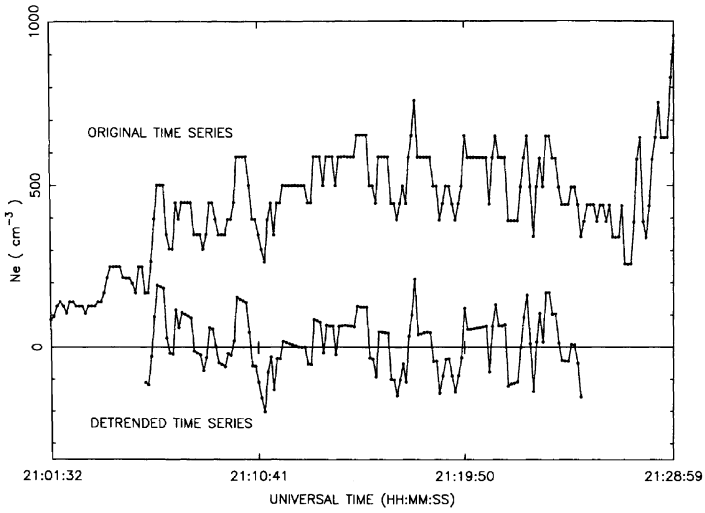

Figure 2. Electron number density profile of the inbound portion of orbit 138. The time series shows data from 2101:32 UT to 2128:59 UT, September 20, 1990.

line in Figure 2. This line gives the density profile from 2101:32 UT to 2128:59 UT on September 20, 1990, immediately following the inbound plasmapause crossing of orbit 138. In order to analyze only the small-scale fluctuations, the longest-period density fluctuations are removed from the density time series by using a detrending process. Fluctuations with periods of 500 s or longer are removed by using an averaging period of 61 data points that corresponds to approximately 500 s in the time series. The arithmetic mean of the first 61 data points is subtracted from the thirtieth point to produce the first detrended point. Next, the mean of the second through the sixty-second points is subtracted from the thirty-first data point to produce the second detrended point. The same process is used with the third through the sixty-third data points and is continued to the end of the time series being analyzed. The values produced by using this "sliding average" of the original time series are interpreted as a measure of the large-scale behavior of the density profile. Subtracting the sliding average values from the original density profile yields a detrended time series with the characteristics of the small-scale fluctuations, as shown in Figure 3. The detrending process using a time period of 500 s acts as a low-pass filter which removes fluctuations with periods of 500 s or greater. The corresponding frequency is approximately 2 mHz, and frequencies lower than this value are filtered out as a result of the detrending process. These detrended data are plotted as the lower line in each of the time series plots and fluctuate about zero. The lower line in Figure 2 shows the density fluctuations corresponding to the density profile of 2101:32 UT to 2128:59 UT on September 20. A peak is present at 2 mHz in all of the power spectra as a result of this detrending process and is ignored unless density structures with periods of about 500 s are clearly present in the time series.

To compute the power spectrum of the density fluctuations, a fast Fourier transform (FFT) is then performed on each density profile. The power spectrum is given by the normalized squares of the FFT coefficients for the profile being analyzed. The maximum frequency plotted is 61.04 mHz, which is the Nyquist frequency corresponding to the SFR sampling rate of 8.192 s. The power spectrum can also be plotted on a log-log scale to test for the presence of well-developed, two-dimensional magnetohydrodynamic (MHD) turbulence. Figure 4 contains an example for the same time period as that shown in Figure 2. The method used to obtain the error spectrum was discussed at the end of the previous section. The power spectrum of two-dimensional turbulence is expected to be the Kolmogorov spectrum, $P \propto k^{-5/3}$ [*Biskamp and Welter*, 1989], where P is the power represented by the FFT coefficients squared and k is the wave number. The spacecraft is assumed to be moving through stationary density structures so that the wave number is proportional to the frequency. The slope of the log-log plot should then have a slope of $-5/3$ if a Kolmogorov

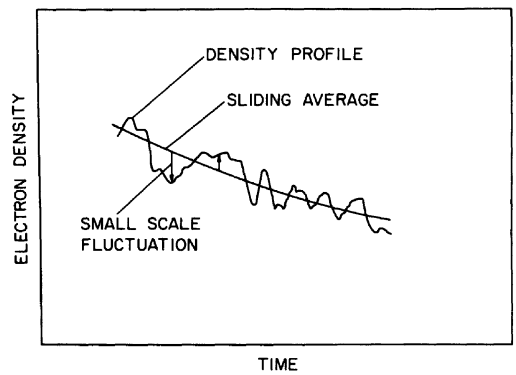

Figure 3. Generalized density profile illustrating the steps in the detrending process.

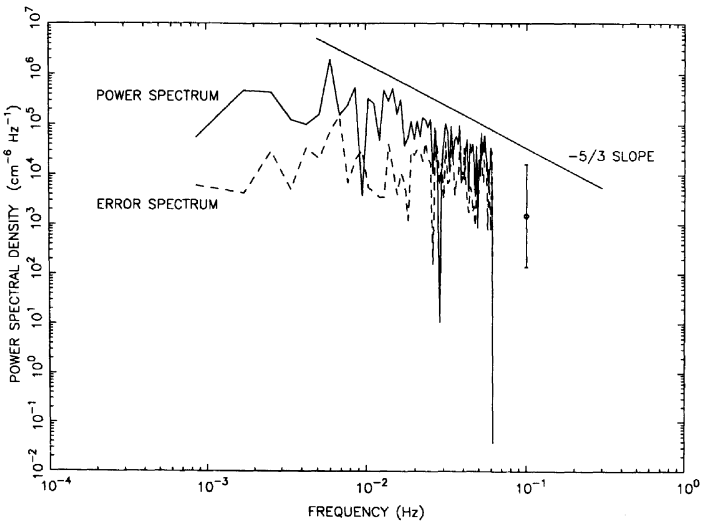

Figure 4. Log-log plot of the power spectrum for the time series from 2101:32 UT to 2128:59 UT, September 20, 1990. The spectral resolution is 0.86 mHz. A line of slope −5/3 is plotted for comparison, and a characteristic error bar is shown.

spectrum is present. A linear plot of the power spectrum is useful for identifying characteristic frequencies that might be present in the observed density fluctuations.

As the first step in the analysis the power spectra are computed directly from the FFT coefficients, with no spectral smoothing or averaging. All details of the original spectrum are shown, and a line with a slope of −5/3 is drawn for comparison to the Kolmogorov spectrum. An example of this step is shown in Figure 4. Spectral smoothing is used to increase the statistical reliability of each component of the power spectrum and is shown in Figure 5 for the time period traced in Figure 2. Spectral smoothing is accomplished by convolving the original power spectrum with a filter function of a specified shape and width [*Sentman*, 1974]. The power spectra in this analysis have been smoothed with a Gaussian filter of width 10 mHz. The statistical reliability of the individual spectral components is increased, and the general trend of the power spectra is shown. The 80% confidence factor is shown in each spectrum for a typical spectral point. The methods used to calculate the power spectra, to perform spectral smoothing, and to provide error bars follow *Spangler et al.* [1988].

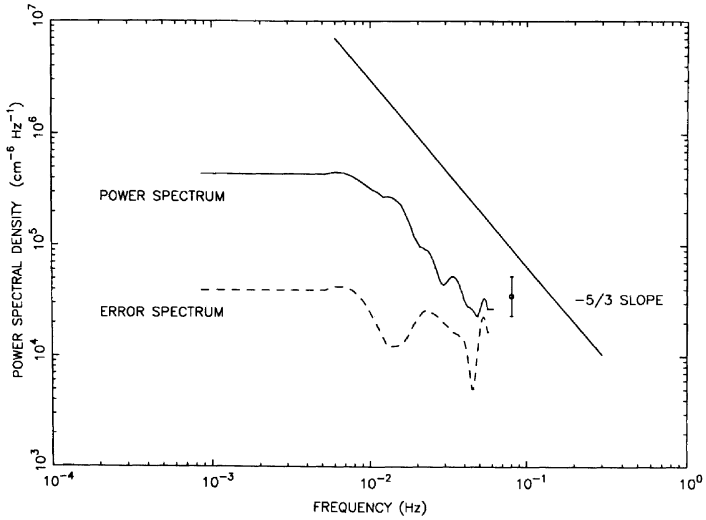

Figure 5. Smoothed power spectrum for the time series from 2101:32 UT to 2128:59 UT, September 20, 1990. The spectral resolution is 10 mHz. A line of slope −5/3 is plotted for comparison, and a characteristic error bar is shown.

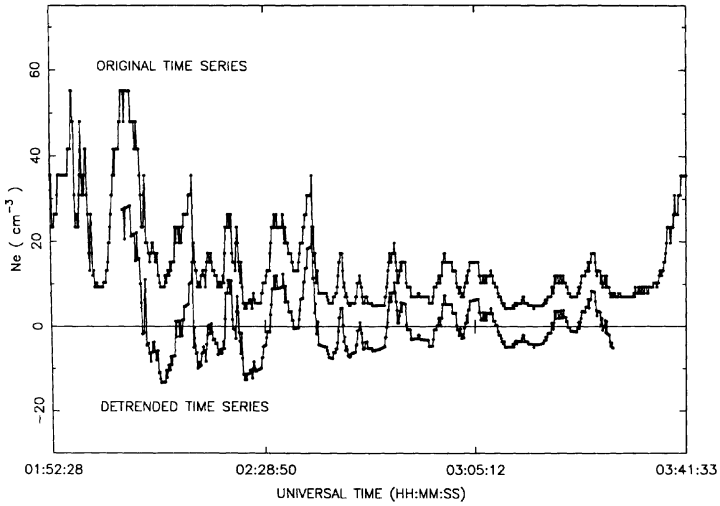

Figure 6. Electron number density profile at apogee of orbit 251. The time series runs from 0152:28 UT to 0341:33 UT, November 6, 1990.

Experimental Results

The power spectral analysis was carried out for several time periods that exhibit clear density fluctuations. The two time periods presented below are examples of the different power spectral behaviors observed in this study. They are labeled by the date and starting time of the spectrogram from which the density profile is traced.

September 20, 1990, 2026 UT

The density profile in Figure 2 shows data obtained from 2101:32 UT to 2128:59 UT on September 20, 1990, during the inbound portion of orbit 138. Density fluctuation amplitudes of approximately 200 cm^{-3} are present during the entire time series. The power spectrum shown by the upper curve in Figure 4 has a slope which is very nearly $-5/3$. This spectrum has a spectral resolution of 0.86 mHz. The error spectrum, shown by the lower curve in Figure 4, is very close to the level of the power spectrum at frequencies greater than 30 mHz. The smoothed spectrum shown in Figure 5 has a spectral resolution of 10 mHz. The slope is again very nearly $-5/3$, so it is likely that two-dimensional MHD turbulence may be occurring during this time series.

November 6, 1990, 0152 UT

The density profile produced on November 6, 1990, from 0152:28 UT to 0341:33 UT during the outbound pass of orbit 251, shown in Figure 6, differs from most of the time periods examined in that the electron density stays relatively constant with a lower average density throughout the entire time period while still containing significant density fluctuations. The spacecraft is outside the plasmasphere during this entire time series. The power spectrum of this time series showed one large peak near 2 mHz when a period of 500 s was used in the detrending process. To determine whether a spectral component not due to the detrending process is present at 2 mHz, this time series was detrended by using a 1500-s time period. The 1500-s detrending period produces the peak near 0.7 mHz in the power spectrum shown in Figure 7. A peak is still present at 2.4 mHz, although the error of a spectral component is greater than the amplitude of the peak. Figure 8 shows the smoothed spectrum with a spectral resolution of 1 mHz. A peak is still present during this time. The average satellite velocity, v_s, can be used to approximate the spatial size of density irregularities with these frequencies. The average spacecraft velocity for this time period is 1.81 km/s. The wavelength for irregularities with this frequency is found by using

$$\lambda = \frac{v_s}{f} \tag{4}$$

Fluctuations with a frequency of 2.4 mHz correspond to a wavelength of approximately 750 km along the spacecraft orbit.

4. Statistical Analysis

The purpose of this statistical analysis is to determine the correlation of the amplitude of the electron density fluctuations with various magnetospheric coordinates such as the McIlwain L parameter and magnetic local time. The electron density data analyzed include all available density data from August 1, 1990, when the sweep frequency receiver was switched on, to December 22, 1990, when the SFR was switched off for several weeks. Traces after this time have not been completed and restrict analysis of local time dependence, as will be discussed later in this section.

Analysis Procedure

The normalized amplitude of density fluctuations is calculated for a time period approximately 5.5 min long. This length of time was chosen so that the change in L shell along the orbit remains less than 0.5. The maximum change in L shell for this period of time is approximately 0.3. The normalized density fluctuation amplitude is calculated by

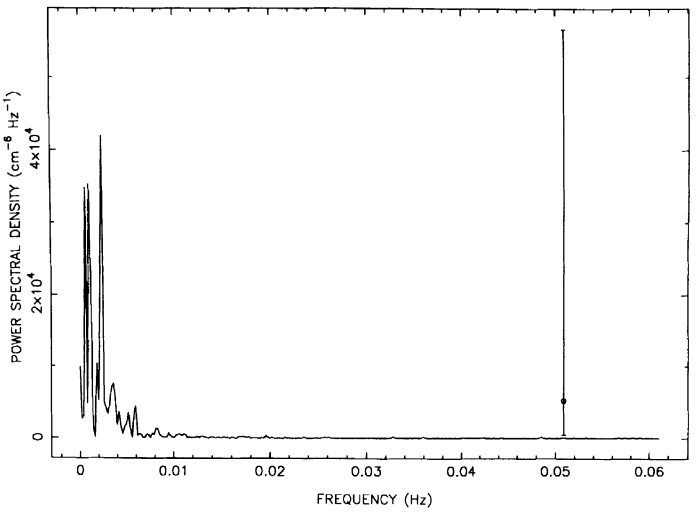

Figure 7. Linear plot of the power spectrum for the time series from 0152:28 UT to 0341:33 UT, November 6, 1990. The spectral resolution is 0.2 mHz.

first finding the standard deviation, σ, of the density values in the first 5.5-min time interval, since this is approximately equal to the root-mean-square average of the density fluctuations during the interval. The standard deviation is then divided by the average density of the time interval. This quantity, $\sigma/\langle x\rangle$, is the coefficient of variation and gives the approximate rms density fluctuation amplitude as a percentage of the average density during the time interval. The coefficient of variation for the electron number density is denoted by $(n_e)_{\rm rms}/\langle n_e\rangle$ on Figures 9 and 10. Subsequent 5.5-min time intervals have 50% overlap. This overlapping is performed to ensure continuous coverage of the data to reduce information loss in the analysis without oversampling the original data. Calculation of the coefficient of variation for these overlapping time intervals continues until the end of the data file. This analysis is then performed on other available data files, and the results are collected in one output file.

Results of the Statistical Analysis

The normalized density fluctuation amplitudes calculated for the data from August 1, 1990, through December 22, 1990, are plotted versus L shell. The scatterplot of these data are shown in Figure 9. The density irregularity amplitudes

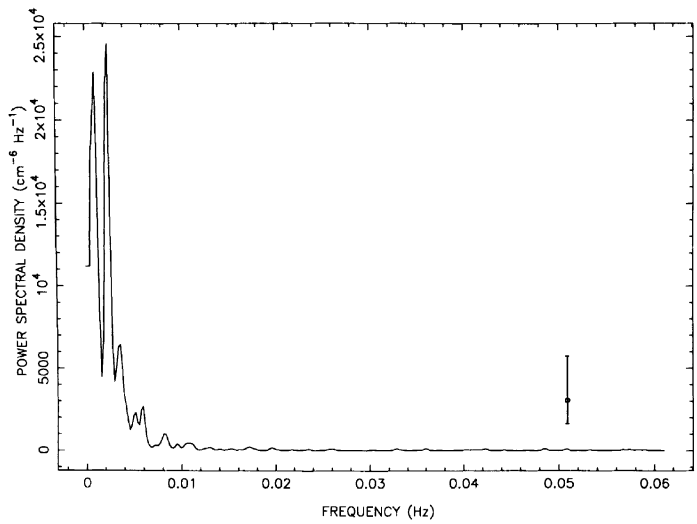

Figure 8. Smoothed power spectrum for the time series from 0152:28 UT to 0341:33 UT, November 6, 1990. The spectral resolution is 1 mHz. A peak is present at 2.4 mHz. A representative error bar is shown.

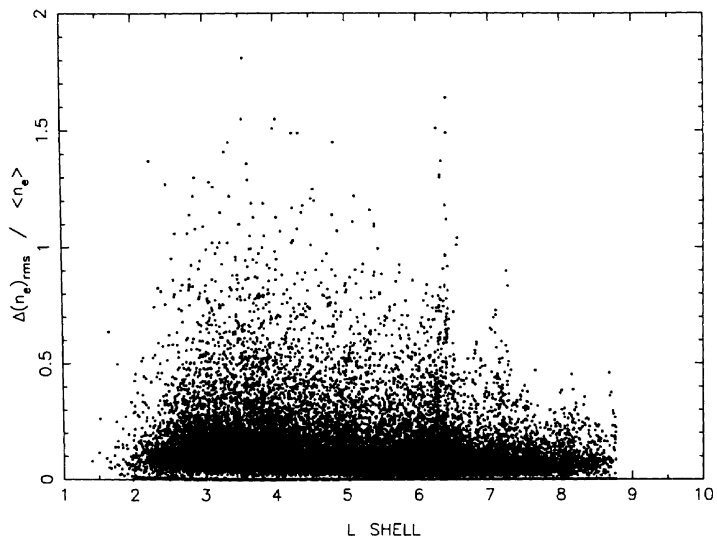

Figure 9. Scatterplot of the normalized rms density fluctuation amplitude as a function of L shell. Maximum irregularity amplitudes occur between $L = 3$ and $L = 5$.

range from 0% (no fluctuation) to almost 200% of the average density during a 5.5-min time interval. Density irregularities of greater than 100% of the average occur in this analysis when the standard deviation is calculated for a series of data containing a steep gradient. If large fluctuations occur while there is a steep gradient in the density over the interval being observed, a standard deviation greater than the average can be obtained. Density fluctuation amplitudes greater than 100% probably occur during the steep density gradients which can be encountered during distinct plasmapause crossings, detached plasma region crossings, or satellite encounters with other density structures.

Figure 9 also shows that the largest fluctuation amplitudes occur for L values between 3 and 5. This result suggests that the largest density irregularities are probably associated with the plasmapause. The maximum density fluctuation amplitudes decrease for L shell values greater than 5; i.e., the density fluctuation amplitude decreases with increasing L shell. Figure 10 shows the same data plotted as quartiles on a logarithmic scale with bins 0.5 L in width from $L = 1$

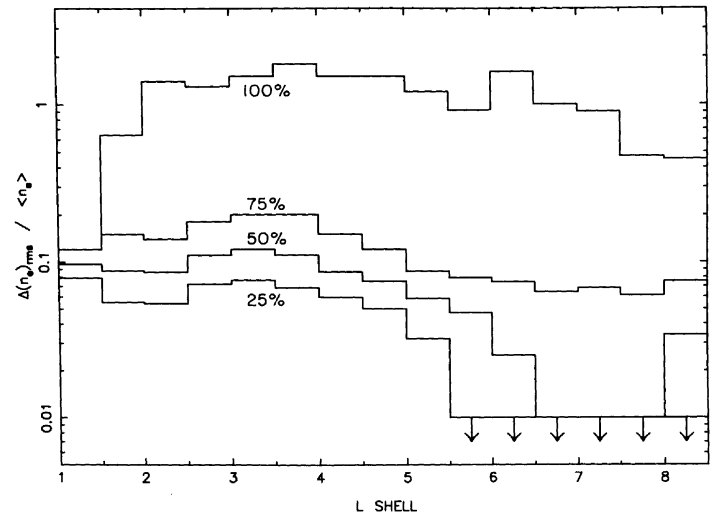

Figure 10. Semilog plot of the normalized rms density fluctuation amplitude quartiles as a function of L shell.

to $L = 8.5$. The maximum density fluctuation amplitude occurs in the $3.5 < L < 4.0$ bin, and the maximum decreases for $L > 4.0$, with the exception of the $6.0 < L < 7.0$ bins. The event which corresponds to this large-amplitude fluctuation will be discussed later in this section. The twenty-fifth, fiftieth, and seventy-fifth percentiles all occur at values much less than the maximum value of the data, and for most of the L shell ranges the twenty-fifth and fiftieth percentiles of the fluctuations measured have amplitudes less than 10% of the average number density. For $L > 5.5$ the twenty-fifth percentile contains fluctuations less than 1% of the average, and for $6.5 < L < 8.0$ the fiftieth percentile also contains fluctuations less than 1% of the average. The seventy-fifth percentile contains fluctuation amplitudes between 10% and 20% of the average density until $L > 5.0$. For greater L values the amplitudes in the seventy-fifth percentile range between 5% and 10%. The one hundredth percentile for all L shell ranges contains fluctuation amplitudes above 10% of the average density. This comparison shows that no more than one quarter of the density data acquired from August through December 1990 contained density fluctuations with amplitudes greater than 10% of the average density. Outside the plasmapause the amplitude of the density fluctuations and the rate of occurrence of significant fluctuations clearly decrease with increasing L.

The large-amplitude fluctuations which produce the spike at $L = 6.4$ in Figure 9 occur during two isolated time periods. A normalized density fluctuation amplitude of 1.18 is calculated from a 5.5-min time period centered at 2040:15 UT on October 3, 1990. At this time the spacecraft was at 5.01 hours magnetic local time (MLT), with a radial distance of 6.24 R_E and an L shell value of 6.39. Several other density fluctuation amplitudes greater than 1.0 are calculated from time intervals which range from 2227:35 UT to 2314:00 UT on October 5, 1990. Three of these occur during consecutive time periods from 2227:35 UT to 2233:02 UT during which the satellite covers a local time range from 5.24 to 5.29 hours. The radial coordinates are $L = 6.41$ and $R = 6.26$ R_E for this time period and do not change appreciably because the satellite is at apogee. A fourth large fluctuation occurs at 2257:37 UT with $L = 6.34$, MLT = 5.55 hours, and $R = 6.18$ R_E. The fifth large fluctuation occurs at 2314:00 UT when the spacecraft was at $L = 6.27$, MLT = 5.72 hours, and $R = 6.10$ R_E. A comparison of these large fluctuations to magnetic activity measured by the Dst index showed no obvious correlation to magnetic storm or substorm activity. Further study is needed to determine the cause of the large density fluctuations for local times at $5.0 <$ MLT < 6.0 and L shell values of $6.0 < L < 6.5$.

A study of the dependence on local time of the number of density fluctuation occurrences and amplitudes of density fluctuations was attempted, but incomplete local time coverage of the traced spectrograms prevents reliable conclusions from being made. For the period of August to December 1990 the fluctuation amplitude values were plotted versus L shell value for four magnetic local time sectors. The local time sectors 21.00–2.99 MLT and 3.00–8.99 MLT contain most of the data shown in Figure 9. Both of these sectors exhibit the same trends found in the original data with the maximum density fluctuation amplitudes occurring between $L = 3$ and $L = 5$ and decreasing with increasing L for $L > 5$. The local time sector 9.00–14.99 MLT has significantly fewer data points than the previous sectors, and the 15.00–20.99 MLT sector has only a small number of data values. This lack of density fluctuation amplitude calculations in some local time sectors is due to incomplete local time coverage of the CRRES orbit between August and December 1990. When the spacecraft nears perigee and higher electron densities, the upper hybrid resonance frequency becomes higher than the 400-kHz frequency band of the SFR, and no f_{UHR} emissions can be detected until the satellite passes perigee and enters lower-density regions on the outbound portion of the orbit. During the August to December 1990 period the orbit perigee advances from 19.91 MLT to 14.15 MLT. Spectrogram traces from CRRES orbits completed during 1991 are necessary to complete the local time coverage of the orbit and to conduct a valid study of local time dependence of density fluctuation amplitudes.

5. Conclusions

Small-scale electron density fluctuations are observed by the CRRES satellite in the magnetosphere near the plasmapause. Power spectral analysis of density profiles that contain data from the outer plasmasphere sometimes have spectra that are similar to the Kolmogorov spectrum. Therefore well-developed two-dimensional MHD turbulence apparently exists in these regions. In other cases, density profiles sometimes produce power spectra that contain well-defined peaks, suggesting the presence of quasi-periodic fluctuations. Electron number densities in these time series range from about 1 cm^{-3} to 1000 cm^{-3}. The density fluctuations have amplitudes up to 200 cm^{-3}. The density fluctuations occur over a range of frequencies, from 2 mHz to almost 61 mHz. The upper limit of detectable density fluctuation frequencies is 61.04 mHz, which corresponds to the smallest density fluctuation period of 16.384 s, which is 2 times the sampling time interval of the upper frequency bands of the CRRES sweep frequency receiver.

The density fluctuations with the largest amplitudes occur between $L = 3$ and $L = 6$, the range in which the plasmapause is found. The density fluctuation amplitude decreases with increasing L for $L > 6$. During the period between August 1, 1990, and December 22, 1990, density fluctuation amplitudes of 10% or greater of the average local electron density were present in only 25% of the data collected. At least half of the available density data contained fluctuations which were 1% or less of the average local density. In the magnetic local time sectors 21.00–2.99 MLT and 3.00–8.99 MLT the distribution of density fluctuation amplitude with respect to L shell is similar to that observed in the full data set. Unfortunately, inadequate coverage of the remaining local time sectors makes a valid study of density fluctuation amplitude dependence on local time impossible.

Density structures in the plasmasphere have been studied recently using the Very Large Array radio-interferometer [*Jacobson and Erickson*, 1993]. The density irregularities observed in this study are called magnetic-eastward-directed (MED) irregularities. Two cosmic radio sources are observed from each of two or three radio antenna pairs. These antenna pairs are located along an axis parallel to the line of motion of the observed density irregularities. The lines of sight of the antennas remain fixed on the radio sources, which move westward across the sky as the Earth rotates.

Density irregularities that are assumed to be located in the corotating plasmasphere will then appear to move eastward across the lines of sight of the antennas. Analysis of the motion of density irregularities across the lines of sight to the radio sources are used to determine the trace speed and altitude of these irregularities. These MED irregularities were originally thought to be located in the ionosphere, but recently they have been determined to occur in the plasmasphere and to corotate with the Earth. These irregularities occur most often in the L shell range $2.0 \lesssim L \lesssim 3.0$. It was also found that the density irregularities in higher L shells were observed at higher magnetic latitudes. The irregularities have wavelengths perpendicular to the magnetic field of approximately 30–40 km and amplitudes of the order of 100 cm^{-3}. These MED irregularities may be part of the same spectrum of density irregularities observed in this spectral analysis, but wavelengths of 30–40 km would appear near or above the Nyquist frequency and would not be clearly seen in these power spectra. The results of the spectral analysis of the CRRES density data showed some density structures with spatial scales along the orbit of approximately 750 km. The electron density fluctuations occur in the L shell range $1.5 < L < 8.5$. Although measurements are taken with magnetic latitude of $\leq 28°$ and the scale length of the structures found in this spectral analysis are larger than the size of the MED irregularities found in the radio-interferometer study, some density structures observed in the CRRES density profiles may coincide with the size of the MED irregularities. This implies that some of the density structures observed by CRRES could be the same as the MED irregularities that are stationary with respect to, and corotating with, the plasmapause.

During approximately 75% of the upper hybrid resonance frequency fluctuation events observed in this study, emissions are also often observed below 100 Hz in the portion of the spectrogram produced by the spectrum analyzer simultaneously with fluctuations in the upper hybrid resonance frequency fluctuations. The low-frequency emissions have the largest amplitudes when the upper hybrid resonance frequency fluctuations are largest, and they occur most often in the outer plasmasphere. These low-frequency waves appear to be associated with, and perhaps are a high-frequency extension of, the density fluctuations we have been studying.

A study of possible mechanisms that produce these density irregularities is beyond the scope of this report, but a few possibilities can be mentioned. *Park and Helliwell* [1971] suggested that lightning discharges produce electric fields perpendicular to geomagnetic field lines. It is postulated that these electric fields are mapped into the plasmasphere along the field lines. The resulting $\mathbf{E} \times \mathbf{B}$ drift then causes flux tubes to rotate about the magnetic field lines. Flux tubes with smaller electron density rotate inward and are replaced by higher-density tubes that are rotating outward. This interchange appears as a fluctuation in a density profile produced by a spacecraft flying through such a structure. Density irregularities could also be produced by MHD waves or plasma depletions in flux tubes caused by ionospheric effects. Finally, two-dimensional MHD turbulence could be caused by a velocity shear at the plasmapause. The plasma inside the plasmapause corotates with the Earth and flows with a velocity relative to the nonrotating plasma outside the plasmapause. This velocity shear will produce a Kelvin-Helmholtz instability at the plasmapause that can evolve into well-developed turbulence.

Acknowledgments. This research was supported by contract 9-X29-D9711-1 with Los Alamos National Laboratory; contract F19628-90K0031 with the United States Air Force, Hanscom Air Force Base; and funds from the University of Iowa Graduate College.

The Editor thanks B. Higel and another referee for their assistance in evaluating this paper.

References

Anderson, R. R., D. A. Gurnett, and D. L. Odem, CRRES plasma wave experiment, *J. Spacecr. Rockets*, *29*, 570, 1992.

Angerami, J. J., and D. L. Carpenter, Whistler studies of the plasmapause in the magnetosphere, 2, Electron density and total tube electron content near the knee in magnetospheric ionization, *J. Geophys. Res.*, *71*, 711, 1966.

Biskamp, D., and H. Welter, Dynamics of decaying two-dimensional magnetohydrodynamic turbulence, *Phys. Fluids B*, *1*, 1964, 1989.

Carpenter, D. L., Whistler studies of the plasmapause in the magnetosphere, 1, Temporal variations in the position of the knee and some evidence on plasma motions near the knee, *J. Geophys. Res.*, *71*, 693, 1966.

Carpenter, D. L., and C. R. Chappell, Satellite studies of magnetospheric substorms on August 15, 1968, 3, Some features of magnetospheric convection, *J. Geophys. Res.*, *78*, 3062, 1973.

Chappell, C. R., Recent satellite measurements of the morphology and dynamics of the plasmasphere, *Rev. Geophys. Space Phys.*, *10*, 951, 1972.

Chappell, C. R., Detached plasma regions in the magnetosphere, *J. Geophys. Res.*, *79*, 1861, 1974.

Chappell, C. R., K. K. Harris, and G. W. Sharp, The morphology of the bulge region of the plasmasphere, *J. Geophys. Res.*, *75*, 3848, 1970.

Chappell, C. R., K. K. Harris, and G. W. Sharp, The dayside of the plasmasphere, *J. Geophys. Res.*, *76*, 7632, 1971.

Chen, A. J., and J. M. Grebowsky, Plasma tail interpretations of pronounced detached plasma regions measured by Ogo 5, *J. Geophys. Res.*, *79*, 3851, 1974.

Chen, A. J., and R. A. Wolf, Effects on the plasmasphere of a time-varying convection electric field, *Planet. Space Sci.*, *20*, 483, 1972.

Grebowsky, J. M., and A. J. Chen, Effects on the plasmasphere of irregular electric fields, *Planet. Space Sci.*, *24*, 689, 1976.

Gurnett, D. A., and L. A. Frank, Thermal and suprathermal plasma densities in the outer magnetosphere, *J. Geophys. Res.*, *79*, 2355, 1974.

Harris, K. K., and G. W. Sharp, OGO-V ion spectrometer, *Trans. IEEE Geosci.*, *GE-7*, 93, 1969.

Higel, B., Small scale structure of magnetospheric electron density through on-line tracking of plasma resonances, *Space Sci. Rev.*, *22*, 611, 1978.

Higel, B., and W. Lei, Electron density and plasmapause characteristics at 6.6 R_E: A statistical study of the GEOS 2 relaxation sounder data, *J. Geophys. Res.*, *89*, 1583, 1984.

Jacobson, A. R., and W. C. Erickson, Observations of electron-density irregularities in the plasmasphere using the VLA radio-interferometer, *Ann. Geophys.*, *11*, 869, 1993.

Johnson, M. H., and J. Kierein, Combined release and radiation effects satellite (CRRES): Spacecraft and mission, *J. Spacecr. Rockets*, *29*, 556, 1992.

Maynard, N. C., and D. P. Cauffman, Double floating probe measurements on S^3-A, *J. Geophys. Res.*, *78*, 4745, 1973.

Mosier, S. R., M. L. Kaiser, and L. W. Brown, Observations of noise bands associated with the upper hybrid resonance by the Imp 6 radio astronomy experiment, *J. Geophys. Res.*, *78*, 1673, 1973.

Park, C. G., and D. L. Carpenter, Whistler evidence of large-scale electron-density irregularities in the plasmasphere, *J. Geophys. Res.*, *75*, 3825, 1970.

Park, C. G., and R. A. Helliwell, The formation of field-aligned irregularities in the magnetosphere, *Radio Sci.*, *6*, 299, 1971.